Geomechanics and Engineering, *Vol. 17, No. 2 (2019) 181-194*
DOI: https://doi.org/10.12989/gae.2019.17.2.181

Stability analysis of slopes under groundwater seepage and application of charts for optimization of drainage design

Dong-ping Deng*, Liang Li[a] and Lian-heng Zhao[b]

School of Civil Engineering, Central South University, Changsha 410075, China

(Received March 16, 2017, Revised December 11, 2018, Accepted January 15, 2019)

Abstract. Due to the seepage of groundwater, the resisting force of slopes decreases and the sliding force increases, resulting in significantly reduced slope stability. The instability of most natural slopes is closely related to the influence of groundwater. Therefore, it is important to study slope stability under groundwater seepage conditions. Thus, using a simplified seepage model of groundwater combined with the analysis of stresses on the slip surface, the limit equilibrium (LE) analytical solutions for two- and three-dimensional slope stability under groundwater seepage are deduced in this work. Meanwhile, the general nonlinear Mohr-Coulomb (M-C) strength criterion is adopted to describe the shear failure of a slope. By comparing the results with the traditional LE methods on slope examples, the feasibility of the proposed method is verified. In contrast to traditional LE methods, the proposed method is more suitable for analyzing slope stability under complex conditions. In addition, to facilitate the optimization of drainage design in the slope, stability charts are drawn for slopes with different groundwater tables. Furthermore, the study concluded that: (1) when the hydraulic gradient of groundwater is small, the effect on slope stability is also small for a change in the groundwater table; and (2) compared with a slope without a groundwater table, a slope with a groundwater table has a larger failure range under groundwater seepage.

Keywords: groundwater seepage; two- and three-dimensional slope stability; limit equilibrium; nonlinear Mohr-Coulomb strength criterion; charts for drainage design

1. Introduction

Many factors could affect the slope stability (Zhang *et al.* 2013, 2015a, b and Peng *et al.* 2018), and groundwater is one of the most important natural factors (Xu *et al.* 2010, Piccinini *et al.* 2014, Luo and Zhang 2016, Zhang *et al.* 2016). In actual engineering, landslides are often caused as a result of the quick rise and poor drainage of groundwater. With the existence and flow of groundwater, the resisting force of a slope would be not only reduced, but its sliding force is also increased, thereby resulting in a significant decline in slope stability (Vandamme and Zou 2013). With respect to the effect on the resisting force of the slope, the normal stress on the slip surface is reduced under the buoyancy of groundwater so as to decrease the shear capacity of the slip surface. For the sliding force of the slope, the downward trend of the slope becomes more obvious under the infiltration force of groundwater. To study the above effects of groundwater on slope stability, the pore water pressure on the slip surface has been involved to calculate the seepage of groundwater in several methods, such as the limit equilibrium (LE) method (Jia *et al.* 2015, Lu *et al.* 2015) and limit analysis (LA) method (Zhang *et al.* 2016).

Using the pore water pressure on the slip surface to show the seepage effect of groundwater is a practical method in the slope stability analysis (Kostic *et al.* 2015, Jelusic *et al.* 2016, Li and Yang 2016, Deng *et al.* 2017). As the calculation of the pore water pressure depends on the shape and location of groundwater table, it is necessary to determine the seepage field of groundwater (Ghiassian and Ghareh 2008). However, the complex groundwater seepage field is usually obtained by numerical simulation with a complicate calculation process, and these obtained results need to be verified by the actual data for judging its applicability. To simplify this analysis process, a previous study used the product of a uniform coefficient (called as the pore water pressure coefficient) and the soil gravity to calculate the pore water pressure on the slip surface (Sun and Zhao 2013). This simplified calculation requires a uniform linear proportional relationship on two vertical heights (one is the vertical height between the groundwater table and slip surface, and another is that between the groundwater table and slope surface), which maybe not accurate with the actual situation. Therefore, it does not accurately reflect the role of groundwater seepage. Here, a simplified model is suggested to establish the groundwater table using some straight lines instead of curved lines so that the analytical solution for the seepage field of groundwater can be easily obtained. In fact, some in-situ monitoring sites are arranged in an actual slope to obtain the groundwater table (Yan *et al.* 2015, Pirone *et al.* 2015), and it is approximately determined by linearly connecting these

*Corresponding author, Lecturer
E-mail dengdp851112@126.com
[a]Professor
E-mail: liliang_csu@126.com
[b]Professor
E-mail: zlh8076@163.com

ISSN: 2005-307X (Print), 2092-6219 (Online)

monitoring sites. Hence, it is feasible to analyze the seepage field of groundwater using this simplified model. Under this simplified model, the calculation of pore water pressure is no longer simply regarded as the product of pore water pressure coefficient and soil gravity, and thus the more reasonable results could be obtained. Moreover, the pore water pressure would be considered as two parts, namely the buoyancy and infiltration force of groundwater, which could be can be calculated analytically in the simplified model. Meanwhile, the location of groundwater table can be described by some parameters in the simplified model of groundwater seepage, such as the highest position of groundwater table.

In addition, the shear strength of soil is also an important factor related to the slope stability. The shear strength of a natural geotechnical body, including the geotechnical body below the groundwater, generally has a nonlinear relationship with the normal stress acting on the geotechnical body (Gao *et al.* 2016, Wang *et al.* 2016). It is only an approximate simplification to replace the nonlinear strength criterion with a linear strength criterion, and the problem of slope stability analysis would become easier under the linear strength criterion. As a simple and practical method, the LE method has been widely adopted by designers to analyze slope stability. However, in the traditional LE methods, it is difficult to obtain the analytical solution of slope stability using the nonlinear strength criterion.

In this work, the simplified model of groundwater seepage is adopted to analyze its effect on slope stability with use of the buoyancy and infiltration force of groundwater on the sliding body. Meanwhile, the shear failure of soil on the slip surface is considered to obey the general nonlinear Mohr-Coulomb (M-C) strength criterion. Then, on the basis of the stress analysis on the slip surface, the LE solutions for two-dimensional (2D) and three-dimensional (3D) slopes under groundwater seepage are deduced. By comparison and analysis on examples, the feasibility of the proposed method is verified. Furthermore, with the highest position of groundwater table as the variables, the slope stability charts under different groundwater tables are drawn. By applying these charts, the stability of slope under the specify groundwater table could be quickly got, and thereby the drainage design in the slope would be guided to satisfy the requirement of slope safety. Moreover, the optimal parameters for the drainage design could be also obtained from these charts.

2. LEM for stability analysis of a slope under groundwater seepage

2.1 LEM for 2D slope stability

As shown in Fig. 1, for a slope with a general shape, the groundwater in the slope is assumed to be flow out at the slope toe. For the highest position of groundwater table, it has the horizontal distance (l_w) and vertical distance (h_w) from the slope vertex. Establishing the *xz* coordinate system with the slope toe as the origin, the equations of the slope surface, slip surface, and groundwater table are $z = g(x)$, $z = s(x)$, and $z = f(x)$, respectively. *A* and *B* are the upper and lower sliding points of slip surface, respectively. In the case of a vertical micro-slice with width dx, it is divides into two parts by the groundwater table. For the part above the groundwater table, the forces acting on it include: the gravity $w_u dx$, the horizontal and vertical seismic forces $k_H w_u dx$ and $k_V w_u dx$, and the horizontal and vertical loads $q_x dx$ and $q_z dx$ on the slope surface. Compared with the part above the groundwater table, the part below the groundwater table would be affected by the buoyancy and infiltration force of groundwater. Thus, on this part, the forces include: the gravity $w_b dx$, the horizontal and vertical forces $k_H w_b dx$ and $k_V w_b dx$, the infiltration force pdx, and the normal and shear stresses $\sigma dx/cos\alpha$ and $\tau dx/cos\alpha$ on slip surface. In the above parameters, k_H and k_V are the horizontal and vertical seismic force coefficients, respectively, p is the infiltration pressure, σ and τ are the normal and shear stresses on slip surface, respectively, and α is the horizontal inclination angle tangent to the slip surface in the vertical micro-slice.

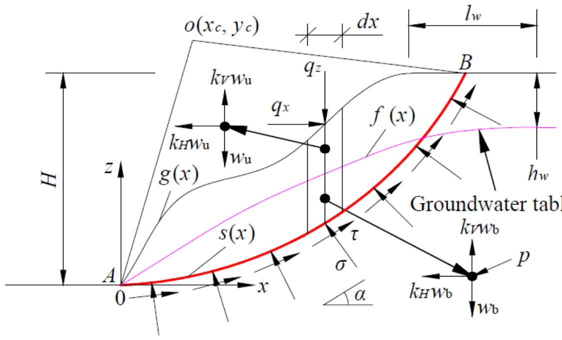

Fig. 1 Model of stability analysis of a 2D slope under groundwater seepage

Here, the slope sliding is considered as the shear failure of slip surface, which is subject to the general nonlinear M-C strength criterion. For the traditional LE method, it is difficult to obtain the analytical solution of slope stability under the nonlinear strength criterion. However, the LE stress method, established by Deng *et al.* (2015, 2016a, 2016b), can be used to analyze the slope stability with the nonlinear strength criterion. Thus, this work derives the LE solution of slope stability under groundwater seepage using the stress assumptions from Deng *et al.* (2015, 2016a, 2016b).

In the LE stress method, the normal stress σ on the slip surface is assumed to be

$$\sigma = \lambda_1 \sigma_0^{2D} \tag{1a}$$

$$\sigma_0^{2D} = \{[(1-k_V)(w_u + w_b) + p_z + q_z)] - [k_H(w_u + w_b) + p_x - q_x]s_x\}/(1+s_x^2) \tag{1b}$$

where σ_0^{2D} is the initial normal stress on the 2D slip surface, which is derived according to the force equilibrium conditions with neglecting the increment of inter-slice forces on the two sides of a vertical micro-slice; λ_1, a dimensionless variable, is the correction coefficient of initial normal stress; $w_u = \gamma(g - f)$; $w_b = (\gamma_{sat} - \gamma_w)(f - s)$; γ is the natural unit weight of soil; γ_{sat} is the saturation unit weight of soil; γ_w is the unit weight of water; p_x and p_z are the components of infiltration pressure along the x and z directions, respectively; $p_x = \gamma_w (f-s)\frac{f_x}{\sqrt{1+f_x^2}}$; $p_z = \gamma_w (f-s)\frac{f_x^2}{\sqrt{1+f_x^2}}$; f_x is the first derivative of groundwater table equation $f(x)$ with respect to the x-axis; s_x is the first derivative of slip surface equation $s(x)$ with respect to x-axis; and $s_x = \tan\alpha$.

In the general nonlinear M-C criterion, the shear strength is

$$\tau_f = c_0 (1+\frac{\sigma}{\sigma_t})^{\frac{1}{m}} \tag{2}$$

where σ is the normal stress of soil; τ_f is the shear strength of soil under the normal stress σ; c_0 is the initial cohesion with $c_0 \geq 0$; σ_t is the uniaxial tensile strength with $\sigma_t \geq 0$; and m is the nonlinear parameter with $m \geq 1$.

For $m = 1$ in Eq. (2), it would represent the linear M-C strength criterion. Then, Eq. (2) can be re-expressed by $\tau_f = c + \sigma\tan\varphi$, where c is the cohesion of soil, φ is the internal friction angle of soil, $c = c_0$, and $\tan\varphi = c_0 / \sigma_t$.

When the slope is in the LE state, the slope factor of safety (FOS) is defined as the ratio of the resisting force on slip surface to the sliding force. For a vertical micro-slice, the FOS can be further simplified as the ratio of the shear strength on slip surface to the shear stress. Thus, using Eq. (2), the shear stress on slip surface can be obtained as

$$\tau = \frac{1}{F_s} c_0 (1+\frac{\sigma}{\sigma_t})^{\frac{1}{m}} \tag{3}$$

where τ is the shear stress on slip surface; and F_s is the FOS of slope.

From Eq. (3), the first derivative of shear stress τ with respect to the normal stress σ on slip surface can be obtained as

$$\frac{d\tau}{d\sigma} = \frac{1}{F_s}\frac{c_0}{m\sigma_t}(1+\frac{\sigma}{\sigma_t})^{\frac{1-m}{m}} \tag{4}$$

Then, expanding Eq. (3) by the Taylor series with the initial normal stress σ_0 as a reference value and substituting Eqs. (4) into the expansion equation, Eq. (3) can be re-expressed as

$$\begin{aligned}\tau = {} & \frac{1}{F_s} c_0 (1+\frac{\sigma_0^{2D}}{\sigma_t})^{\frac{1}{m}} + \\ & \frac{1}{F_s}\frac{c_0}{m\sigma_t}(1+\frac{\sigma_0^{2D}}{\sigma_t})^{\frac{1-m}{m}}(\sigma-\sigma_0^{2D}) + \\ & H(\sigma-\sigma_0^{2D})\end{aligned} \tag{5}$$

where $H(\sigma-\sigma_0^{2D})$ is the higher-order error term.

In Eq. (5), the higher-order error term has correlates with the first two terms on the right-hand side of the equation. Thus, the calculation of $H(\sigma - \sigma_0^{2D})$ can be replaced by linearly amending this two terms. Then, with substitution of Eq. (1a) and introduction of two new variables, the shear stress is assumed as

$$\tau = \lambda_2 \tau_{01}^{2D} + \lambda_3 \tau_{02}^{2D} \tag{6a}$$

$$\tau_{01}^{2D} = c_0 (1+\frac{\sigma_0^{2D}}{\sigma_t})^{\frac{1}{m}} \tag{6b}$$

$$\tau_{02}^{2D} = \frac{c_0}{m\sigma_t}(1+\frac{\sigma_0^{2D}}{\sigma_t})^{\frac{1-m}{m}}\sigma_0^{2D} \tag{6c}$$

where λ_2 and λ_3 are the correction coefficients of shear stress on the slip surface, both of which are dimensionless variables.

As shown in Fig. 1, the force equilibrium conditions in the x and z directions and the moment equilibrium condition of all the forces about the point (x_c, z_c) in the sliding body can be determined as

$$\int[(-\sigma s' + \tau) - k_H (w_u + w_b) - p_x + q_x]dx = 0 \tag{7a}$$

$$\int[(\sigma + \tau s') - (1-k_V)(w_u + w_b) - p_z - q_z]dx = 0 \tag{7b}$$

$$\begin{aligned} & \int[(-\sigma s' + \tau)(y_c - s) + (\sigma + \tau s')(x - x_c)]dx - \\ & \int[(1-k_V)(w_u + w_b) + p_z + q_z](x - x_c)dx - \\ & \int k_H w_u [z_c - \frac{1}{2}(f+g)]dx - \\ & \int (p_x + k_H w_b)[z_c - \frac{1}{2}(s+f)]dx + \\ & \int q_x (z_c - g)dx = 0 \end{aligned} \tag{7c}$$

By substituting Eqs. (7a)-(7b) into Eq. (7c) and simplifying, the following formula can be obtained as

$$\begin{aligned} & \int[\sigma(ss'+x) + \tau(xs'-s)]dx - \\ & \int[(1-k_V)(w_u + w_b) + p_z + q_z]xdx + \\ & \int[\frac{1}{2}k_H w_u (f+g) + \frac{1}{2}(p_x + k_H w_b)(s+f)]dx - \\ & \int q_x g dx = 0 \end{aligned} \tag{8}$$

From Eq. (8), it is noted that the choice of the moment centre point in the sliding body has no effect on the establishment of the LE equations.

Then, by substituting Eqs. (1a) and (6a) into Eqs. (7a)-(7b) and (8), respectively, the following linear equations for the variables λ_1, λ_2, and λ_3 can be obtained as

$$\sum_{j=1}^{3} a_{ij}\lambda_j = b_i \quad (i = 1, 2, 3) \tag{9a}$$

$$a_{11} = -\int \sigma_0^{2D} s' dx \tag{9b}$$

$$a_{12} = \int \tau_{01}^{2D} dx \tag{9c}$$

$$a_{13} = \int \tau_{02}^{2D} dx \tag{9d}$$

$$a_{21} = \int \sigma_{0}^{2D} dx \tag{9e}$$

$$a_{22} = \int \tau_{01}^{2D} s' dx \tag{9f}$$

$$a_{23} = \int \tau_{02}^{2D} s' dx \tag{9g}$$

$$a_{31} = \int \sigma_{0}^{2D} (ss' + x) dx \tag{9h}$$

$$a_{32} = \int \tau_{01}^{2D} (xs' - s) dx \tag{9i}$$

$$a_{33} = \int \tau_{02}^{2D} (xs' - s) dx \tag{9j}$$

$$b_1 = \int [k_H (w_{\mathrm{u}} + w_{\mathrm{b}}) + p_x - q_x] dx \tag{9k}$$

$$b_2 = \int [(1 - k_V)(w_{\mathrm{u}} + w_{\mathrm{b}}) + p_z + q_z] dx \tag{9l}$$

$$\begin{aligned} b_3 = & \int [(1 - k_V)(w_{\mathrm{u}} + w_{\mathrm{b}}) + p_z + q_z] x dx - \\ & \int \frac{1}{2} k_H w_{\mathrm{u}} (f + g) dx - \\ & \int [\frac{1}{2} (p_x + k_H w_{\mathrm{b}})(s + f) - q_x g] dx \end{aligned} \tag{9m}$$

According to Eq. (9), the variables (λ_1, λ_2, and λ_3) would be solved. Thereafter, with substitution of these variables into Eqs. (1)-(6), the normal stress σ and shear stress τ on the slip surface can be obtained.

Based on the above definition, the slope FOS is regarded as the ratio of the resisting force on slip surface to the sliding force for the shear failure of a slope. Thus, the FOS of a 2D slope can be solved using the ratio of the total resisting force along the entire slip surface to the total sliding force, and its formula is

$$F_s = \frac{\int [c_0 (1 + \frac{\sigma}{\sigma_t})^{\frac{1}{m}} / \cos\alpha] dx}{\int (\tau / \cos\alpha) dx} \tag{10}$$

2.2 LEM for 3D slope stability

As shown in Fig. 2(a), in the stability analysis of a 3D slope with slope height H and slope angle β, the symmetry surface of 3D symmetric sliding body (or the main slip surface of 3D asymmetric sliding body) is called the neutral plane. Taking the slope toe in the neutral plane as the origin, an xyz coordinate system is established. Then, $z = g(x, y)$, $z = s(x, y)$, and $z = f(x, y)$ are the equations of slope surface, 3D slip surface, and groundwater table, respectively, where the positive x-axis points into the slope, the positive z-axis is opposite to gravity, and the positive y-axis is determined according to the right hand rule.

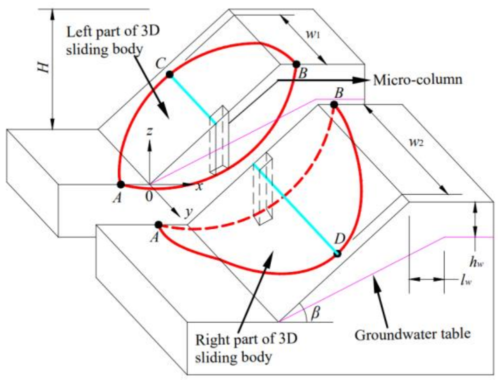

(a) 3D sliding body

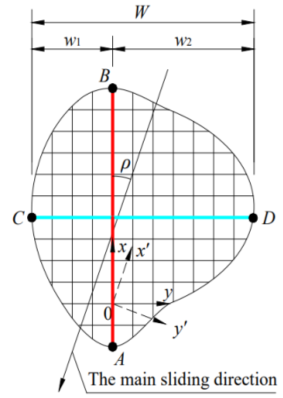

(b) Main sliding direction of 3D sliding body

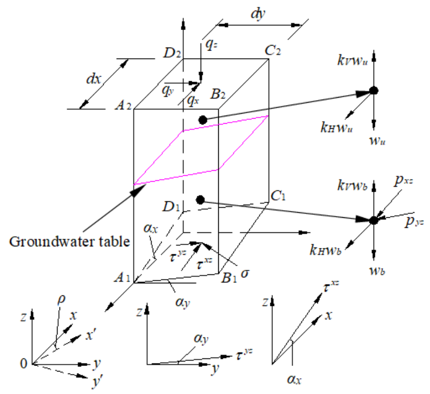

(c) 3D vertical micro-column

Fig. 2 Model of stability analysis of a 3D slope under groundwater seepage

In Fig. 2(a) and 2(b), to describe the characteristics of a 3D sliding body, the width of 3D sliding body along the y-axis is W, and the sliding body is divided into two parts with the neutral plane as the interface. The widths of left and right parts are w_1 and w_2, respectively. Additionally, points A, B, C and D are the upper, lower, left, and right border endpoints of 3D sliding body, respectively, where points A and B are in the neutral plane, and the length of line CD represents the width of 3D sliding body.

In contrast to the simple 2D sliding body, the 3D sliding body slides down substantially along the main sliding direction. For a symmetric sliding body, the main sliding direction is parallel to the symmetry plane (or the neutral plane) because of the symmetry of sliding body. For an asymmetric sliding body, the main sliding direction is not parallel to the neutral plane but is at an angle ρ to the neutral plane. Another coordinate system, i.e., $x'y'z$, is then established with the main sliding direction of 3D sliding body as the x'-axis. Meanwhile, the $x'y'z$ coordinate system has the same origin as the xyz coordinate system, and the positive direction of y'-axis is also determined by the right hand rule. Moreover, the main sliding direction of 3D sliding body is determined by the angle ρ, which can be defined as the inclination angle of the total shear forces on 3D slip surface in the xz plane.

Compared to the original xyz coordinate system, rotating the original coordinate system to align with the main sliding direction of sliding body has the advantage that in the $x'y'z$ coordinate system, only three global LE conditions of 3D sliding body, i.e., the force equilibrium condition in the x' and z directions and the moment equilibrium condition around one point in the y' direction, are required to solve the LE stability of 3D slope. Thus, the complexity of 3D slope stability analysis is reduced, and the calculation speed is improved. Furthermore, the stability of 2D and 3D slopes would be solved by the universal LE equations.

As shown in Fig. 2(c), the vertical 3D micro-column $A_1B_1C_1D_1A_2B_2C_2D_2$ is selected from the 3D sliding body. The micro-column has widths dx and dy in the x and y directions, respectively. α_x and α_y are the inclination angles of slip surface $A_1B_1C_1D_1$ in the xz and yz planes, respectively, where α_y is positive in the clockwise direction along the y-axis and is otherwise negative. Using these parameters, the area of slip surface $A_1B_1C_1D_1$ can be calculated as $\Delta dxdy$, where $\Delta=\sqrt{1+s_x^2+s_y^2}$, $s_x = \tan\alpha_x$, and $s_y = \tan\alpha_y$. Consistent with the vertical 2D micro-slice, the vertical 3D micro-column $A_1B_1C_1D_1A_2B_2C_2D_2$ is also divided into two parts by the groundwater table.

In the vertical micro-column under general conditions, for the part above the groundwater table, the forces acting on it have: the gravity $w_{\mathrm{u}}dxdy$, the horizontal and vertical seismic forces $k_Hw_{\mathrm{u}}dxdy$ and $k_Vw_{\mathrm{u}}dxdy$, and the loads q_xdxdy, q_ydxdy, and q_zdxdy on the slope surface. Moreover, on the part below the groundwater table, the forces include: the gravity $w_{\mathrm{b}}dxdy$, the horizontal and vertical seismic forces $k_Hw_{\mathrm{b}}dxdy$ and $k_Vw_{\mathrm{b}}dxdy$, the infiltration forces $p^{xz}dxdy$ and $p^{yz}dxdy$, the normal stress $\sigma\Delta dxdy$ on slip surface, and the shear stresses $\tau^{xz}\Delta dxdy$ and $\tau^{yz}\Delta dxdy$ on slip surface. In these parameters, p^{xz} and p^{yz} are the components of infiltration pressure in the xz and yz planes. Meanwhile, and τ^{xz} and τ^{yz} are the components of shear stress on slip surface in the xz and yz planes, respectively.

Consistent with the 2D slope stability analysis, the LE stress method assumes the normal stress on the 3D slip surface to be

$$\sigma=\lambda_1\sigma_0^{3D} \tag{11a}$$

$$\begin{aligned}\sigma_0^{3D}=[&\frac{(1-k_V)(w_{\mathrm{u}}+w_{\mathrm{b}})+p_z^{xz}+p_z^{yz}+q_z}{\Delta}-\\&\frac{k_H(w_{\mathrm{u}}+w_{\mathrm{b}})+p_x^{xz}-q_x}{\Delta}\tan\alpha_x+\\&\frac{p_y^{yz}+q_y}{\Delta}\mathrm{sgn}(\alpha_y)\tan\alpha_y]/\\&[n_\sigma^z-n_\sigma^x\tan\alpha_x-n_\sigma^y\mathrm{sgn}(\alpha_y)\tan\alpha_y]\end{aligned} \tag{11b}$$

where σ_0^{3D} is the initial normal stress on 3D slip surface; n_σ^x, n_σ^y, and n_σ^z are the x-, y-, and z-axis direction cosines of normal stress on slip surface, respectively; n_σ^x=-s_x/Δ; n_σ^{xy}=-s_y/Δ; n_σ^z=1/Δ; p_x^{xz} and p_z^{xz} are the components of infiltration force p^{xz} along the x- and z-axis directions, respectively;

$$p_x^{xz}=\gamma_w(f-s)\frac{f_x}{\sqrt{1+f_x^2}};\quad p_z^{xz}=\gamma_w(f-s)\frac{f_x^2}{\sqrt{1+f_x^2}};$$

f_x is the first partial derivative of groundwater table equation $f(x, y)$ with respect to the x-axis; p_y^{yz} and p_z^{yz} are the components of infiltration force p^{yz} along the y- and z-axis directions, respectively;

$$p_y^{yz}=\gamma_w(f-s)\frac{f_y}{\sqrt{1+f_y^2}};\quad p_z^{yz}=\gamma_w(f-s)\frac{f_y^2}{\sqrt{1+f_y^2}};$$

and f_y is the first partial derivative of groundwater table equation $f(x, y)$ with respect to the y-axis.

Similar to the 2D slope, the initial normal stress σ_0^{3D} on slip surface, shown in Eq. (11), is derived according to the force equilibrium conditions when the increment of inter-column forces on the two sides of vertical micro-column is assumed to be zero.

According to the above definition of the angle ρ, it can be solved using the shear stresses τ^{xz} and τ^{yz} on slip surface. For shear stresses τ^{xz} and τ^{yz}, they can be also approximately deduced according to the force equilibrium conditions as the increments of inter-column forces on the two sides of vertical micro-column are neglected. However, in the derivation process of shear stresses, the normal stress on the slip surface should be σ of Eq. (11a) to make the obtained result more reasonable. Thus, the angle ρ is given as

$$\begin{aligned}\rho=\arcsin\{-&\iint(\frac{p_y^{yz}+q_y}{\Delta}+\lambda_1n_\sigma^y\sigma_0^{3D})\Delta dxdy/\\&\iint\sqrt{[\frac{k_H(w_{\mathrm{u}}+w_{\mathrm{b}})+p_x^{xz}-q_x}{\Delta}-\lambda_1n_\sigma^x\sigma_0^{3D}]^2+(\frac{p_y^{yz}+q_y}{\Delta}+\lambda_1n_\sigma^y\sigma_0^{3D})^2}\Delta dxdy\}\end{aligned} \tag{12}$$

The main sliding direction of a 3D sliding body, on the basis of which the $x'y'z$ coordinate system is established, is determined by the angle ρ. Hence, the angle between the planes $x'z$ and xz is also ρ. Thereby, $n_\sigma^{x'}$ and $n_\sigma^{y'}$, which are the x'- and y'-axis direction cosines of normal stress σ on slip surface, respectively, can be calculated as

$$n_\sigma^{x'} = n_\sigma^x \cos\rho + n_\sigma^y \sin\rho \tag{13a}$$

$$n_\sigma^{y'} = -n_\sigma^x \sin\rho + n_\sigma^y \cos\rho \tag{13b}$$

To easily solve for the normal stress σ and the slope FOS (F_s), the visual shear force on slip surface is oriented parallel to the main sliding direction of 3D sliding body, i.e., the visual shear stress τ on slip surface being parallel to the $x'z$ plane. This assumption is widely used in the traditional 3D LE methods. Thereby, the y'-axis direction cosines ($n_\tau^{y'}$) of the visual shear stress τ on slip surface can be calculated as

$$n_\tau^{y'} = 0 \tag{14}$$

For the x'- and z-axis direction cosines of the visual shear stress τ on slip surface in a 3D vertical micro-column, they are named by $n_\tau^{x'}$ and n_τ^z, respectively. Then, these cosines of the normal stress and visual shear stress ($n_\tau^{x'}$, $n_\tau^{y'}$, n_τ^z, $n_\sigma^{x'}$, $n_\sigma^{y'}$, and n_σ^z) have the following relationships as

$$(n_\tau^{x'})^2 + (n_\tau^{y'})^2 + (n_\tau^z)^2 = 1 \tag{15a}$$

$$n_\sigma^{x'} n_\tau^{x'} + n_\sigma^{y'} n_\tau^{y'} + n_\sigma^z n_\tau^z = 0 \tag{15b}$$

By combining Eqs. (13), (14) and (15), the cosines $n_\tau^{x'}$ and n_τ^z can be respectively solved as

$$n_\tau^{x'} = \frac{n_\sigma^z \sqrt{[(n_\sigma^{x'})^2 + (n_\sigma^z)^2]}}{(n_\sigma^{x'})^2 + (n_\sigma^z)^2} \tag{16a}$$

$$n_\tau^z = -\frac{n_\sigma^{x'} n_\tau^{x'}}{n_\sigma^z} \tag{16b}$$

Consistent with the 2D slope stability analysis, the virtual shear stress τ in the 3D slope can be also calculated using Eq. (3) for the slope sliding due to shear failure of slip surface. Thereby, the calculation of the virtual shear stress τ is assumed as

$$\tau = \lambda_2 \tau_{01}^{3D} + \lambda_3 \tau_{02}^{3D} \tag{17a}$$

$$\tau_{01}^{3D} = c_0 (1 + \frac{\sigma_0^{3D}}{\sigma_t})^{\frac{1}{m}} \tag{17b}$$

$$\tau_{02}^{3D} = \frac{c_0}{m\sigma_t} (1 + \frac{\sigma_0^{3D}}{\sigma_t})^{\frac{1-m}{m}} \sigma_0^{3D} \tag{17c}$$

Thereafter, to facilitate the establishment of the LE equations of a 3D sliding body in the $x'y'z$ coordinate system, the x and y coordinates in the 3D vertical micro-column are transformed into their x' and y' coordinates, which are expressed as

$$x' = x\cos\rho + y\sin\rho \tag{18a}$$

$$y' = -x\sin\rho + y\cos\rho \tag{18b}$$

According to the above analysis, only three LE conditions of a 3D sliding body need to be satisfied in the $x'y'z$ coordinate system, i.e., the force equilibrium conditions of all forces acting on a 3D sliding body in the x' and z directions and their moment equilibrium conditions around the point (x_c, y_c, z_c) in the y' direction. Then, they are given as

$$\begin{aligned} &\iint [(\sigma n_\sigma^{x'} + \tau n_\tau^{x'})\Delta - k_H (w_\text{u} + w_\text{b}) \cos\rho] dxdy - \\ &\iint [(p_x^{xz} - q_x) \cos\rho - (p_y^{yz} + q_y) \sin\rho] dxdy = 0 \end{aligned} \tag{19a}$$

$$\begin{aligned} &\iint [(\sigma n_\sigma^z + \tau n_\tau^z)\Delta - (1 - k_V)(w_\text{u} + w_\text{b})] dxdy - \\ &\iint (p_z^{xz} + p_z^{yz} + q_z) dxdy = 0 \end{aligned} \tag{19b}$$

$$\begin{aligned} &\iint (\sigma n_\sigma^z + \tau n_\tau^z)\Delta (x' - x_c) dxdy + \\ &\iint (\sigma n_\sigma^{x'} + \tau n_\tau^{x'})\Delta (z_c - s) dxdy - \\ &\iint (1 - k_V)(w_\text{u} + w_\text{b})(x' - x_c) dxdy - \\ &\iint (p_z^{xz} + p_z^{yz} + q_z)(x' - x_c) dxdy - \\ &\iint k_H w_\text{u} \cos\rho [z_c - (g + f)/2] dxdy - \\ &\iint [(k_H w_\text{b} + p_x^{xz}) \cos\rho [z_c - (f + s)/2] dxdy + \\ &\iint p_y^{yz} \sin\rho [z_c - (f + s)/2] dxdy - \\ &\iint (q_x \cos\rho + q_y \sin\rho)(g - z_c) dxdy = 0 \end{aligned} \tag{19c}$$

By substituting Eqs. (19a) and (19b) into Eq. (19c), Eq. (19c) can be simplified into

$$\begin{aligned} &\iint [\sigma(n_\sigma^z x' - n_\sigma^{x'} s)\Delta + \tau(n_\tau^z x' - n_\tau^{x'} s)\Delta dxdy - \\ &\iint (1 - k_V)(w_\text{u} + w_\text{b}) x' dxdy + \\ &\iint \frac{1}{2} k_H w_\text{u} (g + f) \cos\rho dxdy + \\ &\iint \frac{1}{2} k_H w_\text{b} (f + s) \cos\rho dxdy + \\ &\iint \frac{1}{2} (p_x^{xz} \cos\rho - p_y^{yz} \sin\rho)(f + s) dxdy - \\ &\iint (p_z^{xz} + p_z^{yz}) x' dxdy - \\ &\iint [(q_x \cos\rho + q_y \sin\rho) g + q_z x'] dxdy = 0 \end{aligned} \tag{20}$$

Consist with the 2D analysis, it is also noted from Eq. (20) that the choice of the moment centre point in the 3D sliding body has no effect on the establishment of the LE equations.

By substituting Eqs. (11a) and (17a) into Eqs. (19a)-(19b) and (20), respectively, the linear equations of the three variables λ_1–λ_3 can be obtained as

$$\sum_{j=1}^{3} c_{ij}\lambda_j = d_i \quad (i = 1, 2, 3) \tag{21a}$$

$$c_{11} = \iint \sigma_0^{3D} n_\sigma^{x'} \Delta dxdy \tag{21b}$$

$$c_{12} = \iint \tau_{01}^{3D} n_\tau^{x'} \Delta dxdy \tag{21c}$$

$$c_{13} = \iint \tau_{02}^{3D} n_\tau^{x'} \Delta dxdy \tag{21d}$$

$$c_{21} = \iint \sigma_0^{3D} n_\sigma^{z} \Delta dxdy \tag{21e}$$

$$c_{22} = \iint \tau_{01}^{3D} n_\tau^{z} \Delta dxdy \tag{21f}$$

$$c_{23} = \iint \tau_{02}^{3D} n_\tau^{z} \Delta dxdy \tag{21g}$$

$$c_{31} = \iint \sigma_0^{3D} (n_\sigma^{z} x' - n_\sigma^{x'} s) \Delta dxdy \tag{21h}$$

$$c_{32} = \iint \tau_{01}^{3D} (n_\tau^{z} x' - n_\tau^{x'} s) \Delta dxdy \tag{21i}$$

$$c_{33} = \iint \tau_{02}^{3D} (n_\tau^{z} x' - n_\tau^{x'} s) \Delta dxdy \tag{21j}$$

$$\begin{aligned} d_1 = &\iint [k_H (w_\mathrm{u} + w_\mathrm{b}) + (p_x^{xz} - q_x)] \cos\rho dxdy - \\ &\iint (p_y^{yz} + q_y) \sin\rho] dxdy \end{aligned} \tag{21k}$$

$$\begin{aligned} d_2 = &\iint (1 - k_V)(w_\mathrm{u} + w_\mathrm{b}) dxdy + \\ &\iint (p_z^{xz} + p_z^{yz} + q_z) dxdy \end{aligned} \tag{21l}$$

$$\begin{aligned} d_3 = &\iint [(1 - k_V)(w_\mathrm{u} + w_\mathrm{b}) x' dxdy - \\ &\iint \frac{1}{2} k_H w_\mathrm{u} (g + f) \cos\rho dxdy - \\ &\iint \frac{1}{2} k_H w_\mathrm{b} (f + s) \cos\rho dxdy - \\ &\iint \frac{1}{2} (p_x^{xz} \cos\rho - p_y^{yz} \sin\rho)(f + s) dxdy + \\ &\iint (p_z^{xz} + p_z^{yz}) x' dxdy + \\ &\iint [(q_x \cos\rho + q_y \sin\rho) g + q_z x'] dxdy \end{aligned} \tag{21m}$$

By solving Eq. (21), the variables (λ_1, λ_2, and λ_3) could be obtained. However, according to Eq. (21), the calculation of the parameters (c_{ij} and d_i) in the Eq. (21) is related to the angle ρ. Therefore, the angle ρ should be determined before solving for the variables (λ_1, λ_2, and λ_3). Thus, let the initial value of angle ρ be $\rho^{(0)} = 0$, and these variables (λ_1, λ_2, and λ_3) then is solved using Eq. (21). Thereafter, by substituting the obtained λ_1 into Eq. (12), a new ρ would be calculated. If $|\rho - \rho^{(0)}| \leqq \varepsilon$ (here $\varepsilon = 0.01°$), the obtained values of ρ, λ_1, λ_2, and λ_3 are the final results. If $|\rho - \rho^{(0)}| > \varepsilon$, let $\rho^{(0)} = \rho$, and ρ, λ_1, λ_2, and λ_3 are recalculated. Thereby, the looping iteration of ρ is required to solve for the variables (λ_1, λ_2, and λ_3) in the 3D slope stability.

After the final results of λ_1, λ_2, and λ_3 are obtained, the normal stress σ and visual shear stress τ on 3D slip surface can be calculated by substituting them into Eqs. (11) and (17).

Since the virtual shear stress is assumed to be parallel to the main sliding direction of 3D sliding body, the 3D slope FOS can be also solved using the ratio of the total resisting force on slip surface to the total sliding force, which is consistent with the definition of 2D slope FOS. Then, the 3D slope FOS is calculated as

$$F_s = \frac{\iint c_0 (1 + \frac{\sigma}{\sigma_t})^{\frac{1}{m}} \Delta dxdy}{\iint \tau \Delta dxdy} \tag{22}$$

3. Comparison and analysis of slope examples

3.1 2D slope examples

Taking a 2D homogeneous slope as an example, the influence of groundwater seepage on slope stability is considered. To verify the feasibility of the proposed method, the results of the proposed method are compared with those of the traditional LE methods. The slope height and slope angle are assumed to be H and β, respectively. Moreover, the natural unit weight of soil, saturation unit weight of soil, and unit weight of water are γ, γ_{sat}, and γ_w, respectively, where γ_w = 10 kN/m^3. In the slope, the soil parameter are given as c_0, σ_t, and m under the nonlinear M-C strength criterion, and they would be usually named by the cohesion c and internal friction angle φ if the linear M-C strength criterion (i.e., m = 1 in Eq. (1)) is adopted. Here, for the groundwater table, it is simplified as a straight line, which describes that the groundwater flows from the highest position of groundwater table to the slope toe. l_w and h_w are the horizontal and vertical distances of the highest position of groundwater table from the slope vertex, respectively. Then, according to different combinations of slope parameters, parameters describing groundwater table, and soil parameters, 32 slope examples are formed. Thus, the stability of these slope examples is analyzed by the traditional LE Swedish method (Fellenius 1936), the Morgenstern-Price (M-P) method (Morgenstern and Price 1965), and the proposed method. The calculated results are listed in Table 1. In Table 1, two kinds of slip surface (i.e., circular slip surface and arbitrary curved slip surface) are adopted, and the generation of the arbitrary curved slip surface is from the method of Deng *et al.* (2017). It is well

Table 1 Comparison of the results of 2D slope stability analysis

Examples	Slope parameters		Groundwater table parameters		Soil parameters					Minimum FOS of slope				
										Circular slip surface			Arbitrary curved slip surface	
	H (m)	β (°)	h_w (m)	l_w (m)	γ (kN/m^3)	γ_{sat} (kN/m^3)	c_0 (or c) (kPa)	arctan(c_0/σ_t) (or φ) (°)	m	Swedish method	M-P method	Current method	M-P method	Current method
1	10	30	2	20	17.8	20	25	20	1.0	1.309	1.544	1.558	1.535	1.496
2	10	30	2	20	17.8	20	25	25	1.0	1.474	1.733	1.747	1.726	1.682
3	10	30	2	20	17.8	20	25	30	1.0	1.648	1.933	1.947	1.928	1.878
4	10	30	2	20	17.8	20	25	35	1.0	1.838	2.151	2.163	2.147	2.091
5	10	30	2	20	17.8	20	35	20	1.0	1.591	1.883	1.902	1.867	1.813
6	10	30	2	20	17.8	20	35	25	1.0	1.762	2.08	2.100	2.067	2.012
7	10	30	2	20	17.8	20	35	30	1.0	1.942	2.288	2.307	2.277	2.219
8	10	30	2	20	17.8	20	35	35	1.0	2.138	2.512	2.531	2.503	2.441
9	10	45	2	12	17.8	20	25	20	1.0	1.145	1.231	1.292	1.219	1.259
10	10	45	2	12	17.8	20	25	25	1.0	1.258	1.362	1.425	1.351	1.391
11	10	45	2	12	17.8	20	25	30	1.0	1.380	1.500	1.565	1.489	1.531
12	10	45	2	12	17.8	20	25	35	1.0	1.512	1.649	1.716	1.639	1.682
13	10	45	2	12	17.8	20	35	20	1.0	1.433	1.532	1.614	1.511	1.563
14	10	45	2	12	17.8	20	35	25	1.0	1.552	1.665	1.753	1.650	1.706
15	10	45	2	12	17.8	20	35	30	1.0	1.678	1.811	1.898	1.795	1.851
16	10	45	2	12	17.8	20	35	35	1.0	1.813	1.966	2.055	1.951	2.009
17	10	30	2	20	17.8	20	25	20	1.5	1.043	—	1.254	—	1.182
18	10	30	2	20	17.8	20	25	25	1.5	1.130	—	1.359	—	1.291
19	10	30	2	20	17.8	20	25	30	1.5	1.220	—	1.467	—	1.395
20	10	30	2	20	17.8	20	25	35	1.5	1.314	—	1.579	—	1.506
21	10	30	2	20	17.8	20	35	20	1.5	1.323	—	1.594	—	1.489
22	10	30	2	20	17.8	20	35	25	1.5	1.420	—	1.709	—	1.607
23	10	30	2	20	17.8	20	35	30	1.5	1.519	—	1.826	—	1.728
24	10	30	2	20	17.8	20	35	35	1.5	1.621	—	1.950	—	1.852
25	10	45	2	12	17.8	20	25	20	1.5	0.973	—	1.092	—	1.044
26	10	45	2	12	17.8	20	25	25	1.5	1.037	—	1.169	—	1.123
27	10	45	2	12	17.8	20	25	30	1.5	1.103	—	1.248	—	1.204
28	10	45	2	12	17.8	20	25	35	1.5	1.173	—	1.330	—	1.285
29	10	45	2	12	17.8	20	35	20	1.5	1.264	—	1.413	—	1.340
30	10	45	2	12	17.8	20	35	25	1.5	1.334	—	1.495	—	1.426
31	10	45	2	12	17.8	20	35	30	1.5	1.405	—	1.580	—	1.515
32	10	45	2	12	17.8	20	35	35	1.5	1.480	—	1.670	—	1.607

known that the Swedish method is a non-rigorous method for being only suitable for a circular slip surface, and the M-P method has a rigorous solution without the limitation on the type of slip surface.

Table 1 shows that: (1) compared to the simple LE Swedish method, the proposed method satisfies all the global LE conditions of a sliding body so that a rigorous LE solution is obtained, and it could be also applied with the arbitrary curved slip surface (including the circular slip surface); and (2) the proposed method produces similar results to those of the rigorous LE M-P method, but the proposed method can analyze the slope stability under the nonlinear strength criterion.

3.2 3D slope examples

3D slope example 1: as shown in Fig. 3, is a 3D homogenous slope, with slope height H = 40 m, slope angle β = 45°. The soil parameters γ = 22 kN/m^3, γ_{sat} = 24 kN/m^3, c = 30 kPa, and φ = 30° for the slope subject to the linear M-C strength criterion. Moreover, γ_w = 10 kN/m^3 for the unit weight of water. For this slope, a 3D spheroid is assumed as the sliding body. Then, by establishing an *xyz* coordinate system consistent with Fig. 2, the equation of 3D

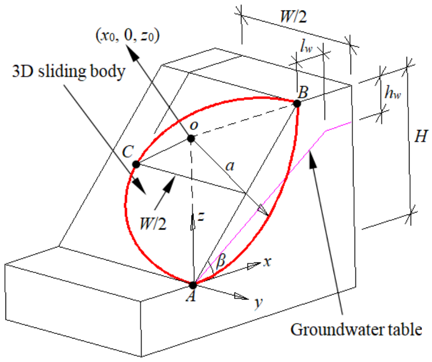

Fig. 3 3D slope example 1

Table 2 Comparison of the results of 3D slope stability analysis

W/H	Slope FOS					
	3D ordinary column method	3D simplified Janbu method	3D Spencer method	3D M-P method	Improved 3D FOS method	Current method
1	1.152	1.252	1.343	1.368	1.480	1.219
2	1.142	1.172	1.237	1.261	1.340	1.192
4	1.142	1.162	1.219	1.232	1.292	1.177
6	1.153	1.142	1.210	1.218	1.260	1.173
8	1.154	1.142	1.209	1.214	1.260	1.172

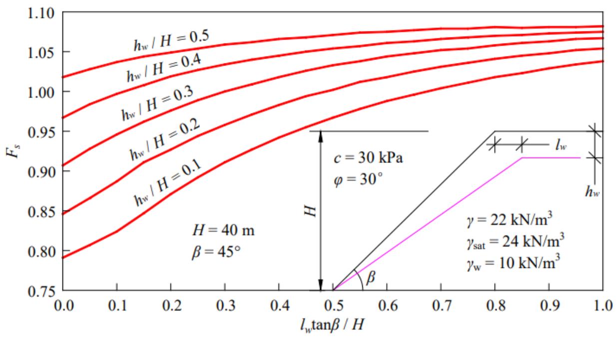

Fig. 4 Results of 3D slope stability analysis for a dynamic change in groundwater

ellipsoid is given as

$$\frac{(x-x_0)^2}{a^2}+\frac{(z-z_0)^2}{a^2}+\frac{y^2}{b^2}=1 \tag{23}$$

where a and b are the shape parameters of 3D ellipsoid, and (x_0, 0, z_0) is the center coordinates of the circular slip surface with radius a in the neutral plane of 3D sliding body.

In Eq. (23), the parameter b can be determined on basic of the parameters x_0, z_0, a, H, β, and W (i.e., the width W of 3D sliding body) as

For $x_0 < -z_0\tan\beta$ and $x_0 < 0$,

$$b=\frac{W}{2\sqrt{1-\frac{z_0^2}{a^2}}} \tag{24a}$$

For $x_0 > H/(\sin\beta\cos\beta) - z_0\tan\beta$ and $x_0 > H/\tan\beta$,

$$b=\frac{W}{2\sqrt{1-\frac{(H-z_0)^2}{a^2}}} \tag{24b}$$

For other cases,

$$b=\frac{W}{2\sqrt{1-(\frac{x_0}{a}\tan\beta-\frac{z_0}{a})^2/[1+\tan^2\beta]}} \tag{24c}$$

To compare the results with other methods, the slope without the groundwater table is given, and the 3D ellipsoid is also used with the parameters of the sliding body as x_0 = 40 m, z_0 = 40 m, and a = 40 m at the specific position. Then, the FOS of a 3D slope for W/H =1, 2, 4, 6, and 8 is calculated, and the results are listed in Table 2. Table 2 shows that the proposed method has the close results with the 3D simplified Janbu method (Hungr 1989), 3D Spencer method (Zhang 1988), and 3D M-P method (Cheng and Yip 2007), thereby verifying the feasibility of the proposed feasibility. Moreover, similar to the 3D ordinary column method (Hovland 1997), only three LE conditions of a 3D sliding body are adopted in the proposed method. However, the proposed method obtains the global LE conditions of a 3D sliding body from the special Cartesian coordinate system, which is established on the basis of the main sliding

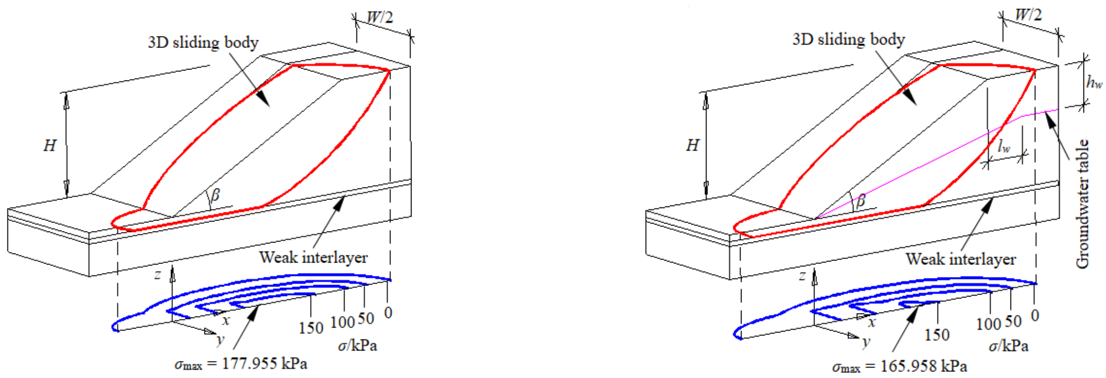

(a) Slope without groundwater table (b) Slope under groundwater seepage

Fig. 5 Contrast on the results of critical slip surface and normal stress on slip surface in 3D slope example 2

direction of 3D sliding body. Thus, the rigorous 3D LE solutions can be solved by the proposed method. In addition, the improved 3D FOS method (Wang and Deng 2003) has a larger FOS than the proposed method for the reason that it considers the appearance of sliding between the adjacent 3D vertical columns. In fact, a relative displacement between the adjacent 3D vertical columns may be not obvious when the slope slides due to shear failure of slip surface. Therefore, compared with the improved 3D FOS method, the results obtained by the proposed method are more conservative.

For the slope with the consideration of groundwater table, the effect of a dynamic change in the groundwater table on slope stability is studied. To easily describe the groundwater seepage in a 3D slope, it is assumed that the groundwater flows out from the slope toe, and the groundwater table between its highest position and the slope toe is simplified into a plane, which is the same with the simplified seepage model for a 2D slope. For the highest position of groundwater table, l_w and h_w are its horizontal and vertical distances from the slope vertex, respectively. Meanwhile, no hydraulic gradient acts on this simple 3D slope along the y-axis direction, that is, the seepage does not occur along the width direction of a 3D sliding body. Then, the above 3D rotating ellipsoid with the same parameters is also adopted as the sliding body to analyze the slope stability. Thus, when W = 20 m, the curves of the minimum FOS of 3D slope vs. the parameter $(l_w \tan\beta) / H$ are plotted for h_w / H = 0.1, 0.2, 0.3, 0.4, and 0.5 in Fig. 4.

Fig. 4 shows that: (1) the slope stability would be reduced under the groundwater seepage, and the slope tends to be more likely instability with the high groundwater table; and (2) a change in the groundwater table would has the small effect on the slope stability under the condition of the low hydraulic gradient of groundwater, and the hydraulic gradient is expressed by $(H - h_w) / (H / \tan\beta + l_w)$.

3D slope example 2: as shown in Fig. 5, the 3D slope with a weak interlayer has slope height H = 12.25 m and slope ratio 1:2, i.e., slope angle β = 26.565°. The weak interlayer is located below the slope toe with the vertical distance h_d = 0.75 m, and its thickness is h = 0.5 m. The soil parameters are γ = 18.84 kN/m^3, γ_{sat} = 21 kN/m^3, c = 28.5 kPa, and φ = 20° for the slope subject to the linear M-C strength criterion. γ_w = 10 kN/m^3 for the unit weight of water. For the weak interlayer, which is also subject to the linear M-C criterion, it has γ = 18.84 kN/m^3, γ_{sat} = 21 kN/m^3, c = 0.0 kPa, and φ = 10°. Similar to the 3D slope in example 1, the 3D rotating ellipsoid as the sliding body is also adopted in this example. However, the presence of a weak interlayer makes it easier for the slope to slide along its surface. Thus, when the 3D rotating ellipse is below the weak interlayer, it would be replaced by the surface of weak interlayer, thereby forming a 3D composite slip surface. Taking the width of 3D sliding body W = 40 m as an example shown in Fig. 5, the minimum slope FOS, the critical slip surface, and the normal stress on the slip surface are respectively calculated for the two cases, i.e., the slope without groundwater and the slope under groundwater seepage. For the slope under groundwater seepage, the groundwater table is simplified using the same model as in 3D slope example 1. Here, $h_w = 0.4H$ and $l_w = 1.2H / \tan\beta$. By analyzing the slope stability, the minimum slope FOS is equal to 2.400 for a slope without a groundwater table, and it is 2.055 for the slope under groundwater seepage conditions. Thus, the slope stability under groundwater seepage is significantly reduced, and it also shows that the groundwater is an important natural factor resulting in slope instability.

Fig. 5 illustrates that the normal stress on the slip surface is obviously reduced by the buoyancy force of groundwater, and as a result the resisting force of slope is also decreased. Meanwhile, the infiltration force of groundwater increases the sliding force of slope so as to reduce significantly the slope stability. In addition, the slope under groundwater seepage has a larger failure range than that without the groundwater table.

4. Charts for optimization of the design of slope drainage

The above analysis shows that the slope stability is significantly reduced with the existence of groundwater seepage. Hence, in the actual engineering scenarios under groundwater table, the drainage is required by arranging some pipes (i.e., drainage pipe) in the slope to improve the slope stability. In other words, it is very important for drainage design in slope under the groundwater seepage. For the drainage pipe, the plastic pipe commonly used in

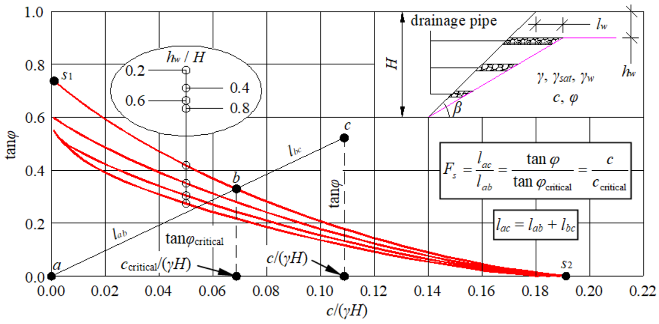

(a) $l_w\tan\beta / H = 0.0$

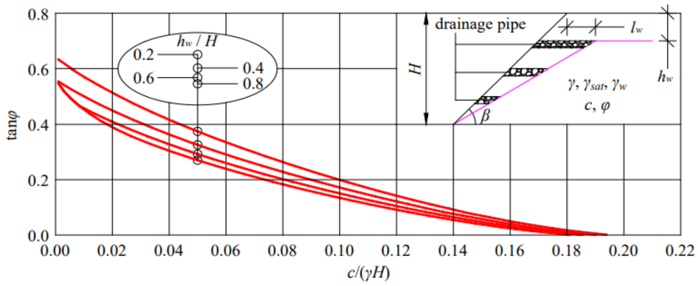

(b) $l_w\tan\beta / H = 0.2$

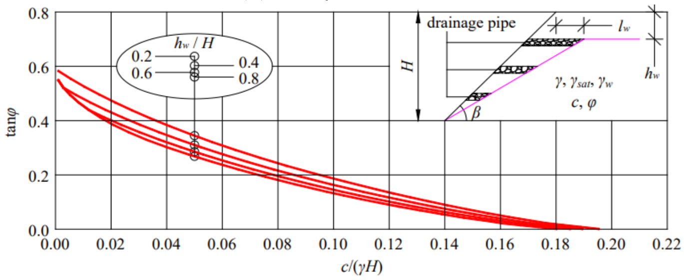

(c) $l_w\tan\beta / H = 0.4$

Fig. 6 Stability charts for optimizing slope drainage design with slope angle β = 30°

the engineering could be adopted, and some drain holes would be set around its shell. Moreover, the mesh geo-textile is wrapped at the end of the pipe and around the shell of the pipe to prevent the silt from entering the pipe. Meanwhile, the drain pipe is arranged obliquely downward within the slope so that the water inside the pipe can quickly flow out under the action of its gravity. With regard to the spacing of the drainage pipes, it can be ensured that the groundwater above the drainage pipes and between the two adjacent drainage pipes should be effectively and promptly discharged.

In addition, compared with the non-linear strength criterion, the linear M-C strength criterion is still widely used by designers for the slope stability analysis. The reason is that only two shear strength parameters included in the linear M-C strength criterion can be quickly and simply obtained by the laboratory experiments and the failure behavior of slope sliding can be also approximately simulated with the use of them. Therefore, it is practical to draw the stability charts of slope with the linear M-C strength criterion for optimizing the design of drainage.

Then, the stability charts of slope are drawn with slope height H = 10 and slope angle β. In the slope, the soil parameters are γ = 17.8 kN/m^3 and γ_{sat} = 20 kN/m^3. γ_w = 10 kN/m^3 for the unit weight of water. Here, it is thought that the groundwater table would descend to the designed position under the work of the drainage system after the drainage pipes are arranged in the slope. Thus, to facilitate designing the position of drainage pipes, the groundwater around the pipes would be drained by them, and finally a new stable groundwater table is formed in the slope. Meanwhile, the new groundwater table can be approximately described using the above simplified model, in which the groundwater undergoes the linear flow from the highest position of groundwater table to the slope toe after drainage. Then, the designed highest position of groundwater table is determined by the parameters l_w and h_w. Thereby, the drainage design of slope is considered as the design of parameters describing the groundwater table, and the purpose of arranging the drainage pipe in the slope is to descend the groundwater table to the designed position.

In the work of Sun and Zhao (2013), the curve of tanφ vs. $c/(\gamma H)$ for the slope in the critical state was plot to form the simple and practical stability charts, and it could be also used to get the stability charts under the different groundwater table for optimizing the drainage design. In the stability charts, a slope in the critical state has the minimum FOS of 1.000, which is used to judge whether the slope is in a stable state. For example, for one point above the curve of tanφ vs. $c/(\gamma H)$, its minimum FOS would be greater than 1.000 and the slope is in a stable state, otherwise, the slope state is unstable with the minimum FOS being less than

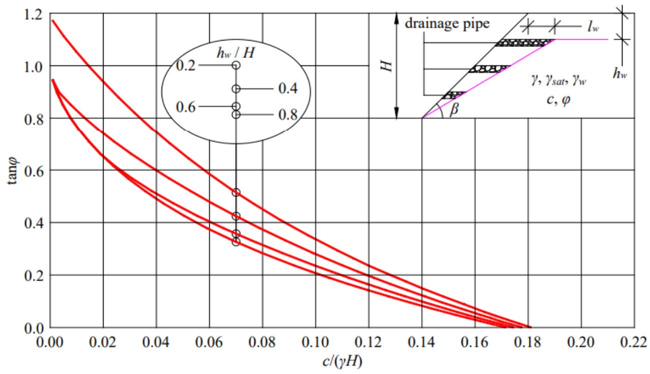

(a) $l_w\tan\beta$ / H = 0.0

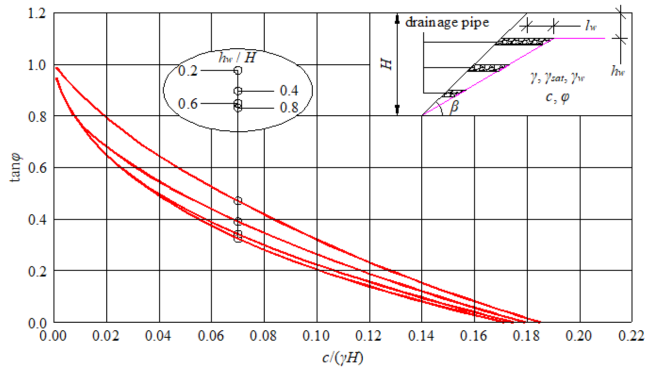

(b) $l_w\tan\beta$ / H = 0.2

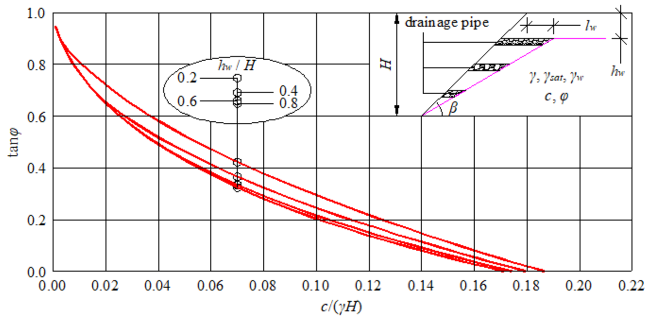

(c) $l_w\tan\beta$ / H = 0.4

Fig. 7 Stability charts for optimizing slope drainage design with slope angle β = 45°

Table 3 Comparison of the calculated results

Case	Slope parameters		Soil parameters					Drainage parameters		Designed minimum FOS of slope	Calculated minimum FOS of slope
	H(m)	β(°)	γ(kN/m^3)	γ_{sat}(kN/m^3)	γ_w(kN/m^3)	c(kPa)	φ(°)	$l_w\tan\beta/H$	h_w/H		
1	10	45	17.8	20	10	18	20	0.0	0.576	1.200	1.202
2	10	45	17.8	20	10	18	20	0.2	0.509	1.200	1.207
3	10	45	17.8	20	10	18	20	0.4	0.415	1.200	1.202

1.000. In addition, when a specific slope is given with different strength parameters, its minimum slope FOS can also solved by a simple linear proportional relationship in the stability charts, which is shown in Fig. 6(a) for the example of β = 30°, h_w / H = 0.2, and ($l_w\tan\beta$) / H = 0.0 with curve s_1s_2.

Here, Figs. 6, 7, and 8 is suitable for h_w / H = 0.2 ~ 0.8 and ($l_w\tan\beta$) / H = 0.0 ~ 0.4, and the application range of slope angle (β) is 30° ~ 60°.

To verify the applicability of these charts for the optimization of slope drainage design, the slope parameters are given as slope height H = 10 m and slope angle β = 45°. In the slope, the soil parameters are γ = 17.8 kN/m^3, γ_{sat} = 20 kN/m^3, c = 18 kPa, and φ = 20°. γ_w = 10 kN/m^3 for the unit weight of water. Meanwhile, the slope under groundwater seepage is in the unstable state. To improve the slope stability, the drainage pipes are arranged in the slope to descend the groundwater table, and the minimum slope FOS would be required to reach 1.200. Thus, according to the given slope and soil parameters, the drainage parameters, i.e., the highest position of groundwater table, are inversely calculated for the

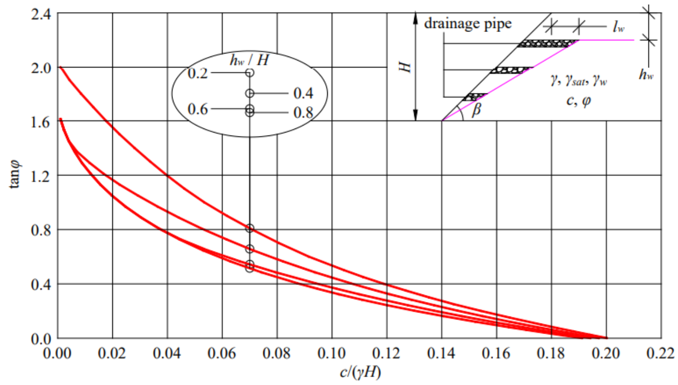

(a) $l_w\tan\beta$ / H = 0.0

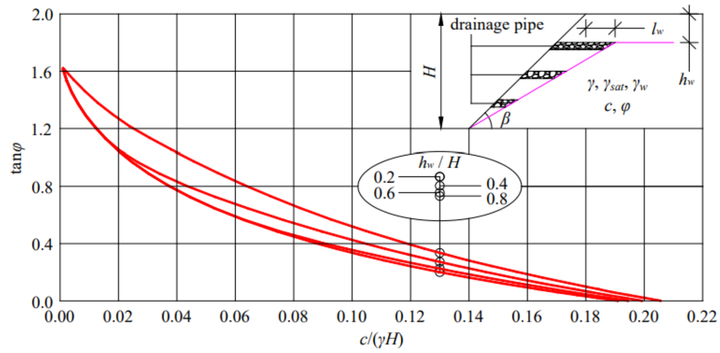

(b) $l_w\tan\beta$ / H = 0.2

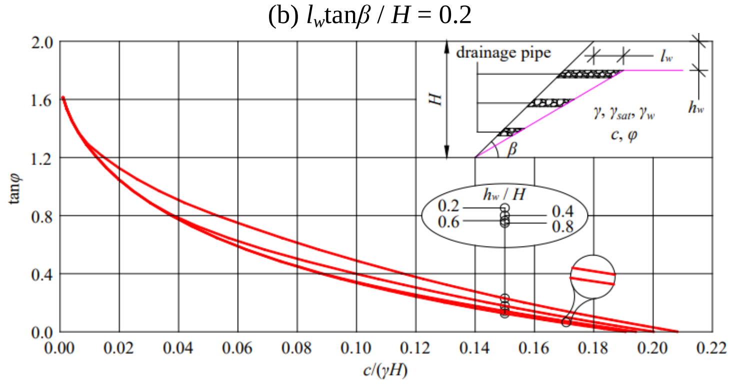

(c) $l_w\tan\beta$ / H = 0.4

Fig. 8 Stability charts for optimizing slope drainage design with slope angle β = 60°

corresponding minimum slope FOS of 1.200. The results are listed in Table 3. Furthermore, the slope stability with the designed drainage parameters is re-analyzed, and the results are also presented in Table 3.

Table 3 shows that it is feasible to design the drainage parameters of slope using these charts in Figs. 6-8, and the designed minimum slope FOS is very close to the calculated value. Thus, with the use of the charts in Figs. 6-8, it could not only quickly get the slope stability under groundwater seepage but obtain the optimal parameters of drainage design for the slope with specific safety requirements.

5. Conclusions

In this work, the slope stability under the groundwater seepage is studied. Here, to obtain easily the infiltration and buoyancy forces of the groundwater on the sliding body, its seepage model is reasonably simplified. Then, by combining the stress analysis on the slip surface, the LE solutions for the stability of 2D and 3D slopes under groundwater seepage are derived with the general nonlinear M-C strength criterion. By comparing the results on some slope examples, the feasibility of the proposed method is verified. Furthermore, the research shows that:

(1) Under the condition of the low hydraulic gradient of groundwater, a change in the groundwater table would have the small effect on the slope stability.

(2) For the slope under groundwater seepage, its stability is significantly reduced for the reason of the decease in the normal stress on slip surface from the effect of buoyancy force and the increase in the sliding force of slope from the effect the infiltration force, and its failure range would also become larger.

(3) The drawn stability charts can be used to quickly obtain the slope stability under groundwater seepage and also to optimize the drainage parameters for the slope with

specific safety requirements.

Acknowledgements

The research described in this paper was financially supported by the National Natural Science Foundation of China (No. 51608541), the China Postdoctoral Science Foundation (No. 2015M580702), and the Guizhou Provincial Department of Transportation, China (No. 2014122006).

References

Cheng, Y.M. and Yip, C.J. (2007), "Three-dimensional asymmetrical slope stability analysis extension of Bishop's, Janbu's, and Morgenstern-Price's techniques", *J. Geotech. Geoenviron. Eng.*, **133**(12), 1544-1555.

Deng, D.P., Li, L. and Zhao, L.H. (2017), "LEM for stability analysis of 3D slopes with general-shaped slip surfaces", *Int. J. Geomech.*, **17**(10), 06017017.

Deng, D.P., Li, L., Wang, J.F. and Zhao L.H. (2016a), "Limit equilibrium method for rock slope stability analysis by using the generalized Hoek-Brown criterion", *Int. J. Rock Mech. Min. Sci.*, **89**(11), 176-184.

Deng, D.P., Li, L., Zhao, L.H. (2017), "Method of generation and model of calculation of arbitrary curved slip surfaces for three-dimensional convex and concave slopes", *Int. J. Geomech.*, **17**(11), 04017095.

Deng, D.P., Zhao, L.H. and Li, L. (2015), "Limit equilibrium slope stability analysis using the nonlinear strength failure criterion", *Can. Geotech. J.*, **52**(4), 563-576.

Deng, D.P., Zhao, L.H. and Li, L. (2016b), "Limit equilibrium method for slope stability based on assumed stress on slip surface", *J. Central South Univ.*, **23**(11), 2972-2983.

Fellenius, W. (1936), "Calculation of the stability of earth dams", *Proceedings of the 2nd Congress on Large Dams*, Washington, D.C., U.S.A.

Gao, Y.F., Wu, D., Zhang, F., Lei, G.H., Qin, H.Y. and Qiu, Y. (2016), "Limit analysis of 3D rock slope stability with non-linear failure criterion", *Geomech. Eng.*, **10**(1), 59-76.

Ghiassian, H.,and Ghareh, S. (2008), "Stability of sandy slopes under seepage conditions", *Landslides*, **5**(4), 397-406.

Hovland, H.J. (1997), "Three-dimensional slope stability analysis method", *J. Geotech. Eng. Div.*, **103**(9), 971-986.

Hungr, O., Salgado, F.M. and Byrne, P.M. (1989). "Evaluation of a three dimensional method of slope stability analysis", *Can. Geotech. J.*, **26**(4), 679-686.

Jelusic, P., Zlender, B. and Dolinar, B. (2016), "NLP optimization model as a failure mechanism for geosynthetic reinforced slopes subjected to pore-water pressure", *Int. J. Geomech.*, **16**(5), C4015003.

Jia, N., Yang, Z.H., Xie, M.W., Mitani, Y. and Tong, J.X. (2015), "GIS-based three-dimensional slope stability analysis considering rainfall infiltration", *Bull. Eng. Geol. Environ.*, **74**(3), 919-931.

Kostic, S., Vasovic, N. and Sunaric, D . (2015), "A new approach to grid search method in slope stability analysis using Box-Behnken statistical design", *Appl. Math. Comput.*, **256**(C), 425-437.

Li, Y.X. and Yang, X.L. (2016), "Stability analysis of crack slope considering nonlinearity and water pressure", *KSCE J. Civ. Eng.*, **20**(6), 2289-2296.

Lu, L., Wang, Z.J., Song, M.L. and Arai, K. (2015), "Stability analysis of slopes with ground water during earthquakes", *Eng. Geol.*, **193**(7), 288-296.

Luo, F.Y. and Zhang, G. (2016), "Progressive failure behavior of cohesive soil slopes under water drawdown conditions", *Environ. Earth Sci.*, **75**(11), 1-12.

Morgenstern, N.R. and Price, V.E. (1965), "The analysis of the stability of general slip surfaces", *Géotechnique*, **15**(1), 79-93.

Peng, X.Y., Yu, P.C., Zhang, Y.B. and Chen, G.Q. (2018), "Applying modified discontinuous deformation analysis to assess the dynamic response of sites containing discontinuities", *Eng. Geol.*, **246**(11), 349-360.

Piccinini, L., Berti, M., Simoni, A., Bernardi, A.R., Ghirotti, M., and Gargini, A. (2014), "Slope stability and groundwater flow system in the area of Lizzano in Belvedere (Northern Apennines, Italy)", *Eng. Geol.*, **183**, 276-289.

Pirone, M., Papa, R., Nicotera, M.V. and Urciuoli, G. (2015), "In situ monitoring of the groundwater field in an unsaturated pyroclastic slope for slope stability evaluation", *Landslides*, **12**(2), 259-276.

Sun, J.P. and Zhao, Z.Y. (2013), "Stability charts for homogenous soil slopes", *J. Geotech. Geoenviron. Eng.*, **139**(12), 2212-2218.

Vandamme, J. and Zou, Q.P. (2013), "Investigation of slope instability induced by seepage and erosion by a particle method", *Comput. Geotech.*, **48**(3), 9-20.

Wang, Y.X. and Deng, H.K. (2003), "An improved method for three-dimensional slope stability analysis", *Chin. J. Geotech. Eng.*, **25**(5), 611-614 (in Chinese).

Wang, Y.Z., Liu, X.F., Zhang, Z.K. and Yang, P.B. (2016), "Analysis on slope stability considering seepage effect on effective stress", *KSCE J. Civ. Eng.*, **20**(6), 2235-2242.

Xu, Q.J., Lu, Y., Yin, H.L. and Li, Z.K. (2010), "Shakedown analysis of a slope with cyclic groundwater level", *Int. J. Numer. Anal. Meth. Geomech.*, **34**(5), 517-531.

Yan, J.F., Shi, B., Zhu, H.H., Wang, B.J., Wei, G.Q., and Cao, D.F. (2015), "A quantitative monitoring technology for seepage in slopes using DTS", *Eng. Geol.*, **186**(2), 100-104.

Zhang, F., Leshchinsky, D., Baker, R., Gao, Y.F. and Leshchinsky, B. (2016), "Implications of variationally derived 3D failure mechanism", *Int. J. Numer. Anal. Meth. Geomech.*, **40**(8), 2514-2531.

Zhang, X. (1988), "Three-dimensional stability analysis of concave slopes in plan view", *J. Geotech. Eng.*, **114**(6), 658-671.

Zhang, Y,B., Zhang, J., Chen, G.Q., Zheng, L. and Li, Y.G. (2015b), "Effects of vertical seismic force on initiation of the Daguangbao landslide induced by the 2008 Wenchuan earthquake", *Soil Dyn. Earthq. Eng.*, **73**(6), 91-102.

Zhang, Y.B., Chen, G.Q., Zheng, L., Li, Y.G., Wu, J. (2013), "Effects of near-fault seismic loadings on run-out of large-scale landslide: A case study", *Eng. Geol.*, **166**(11), 216-236.

Zhang, Y.B., Wang, J.M., Xu, Q., Chen, G.Q., Zhao, J.X., Zheng, L., Han, Z. and Yu, P.C. (2015a), "DDA validation of the mobility of earthquake-induced landslides", *Eng. Geol.*, **194**(8), 38-51.

Zhang, Y.J., Nian, T.K., Zheng, D.F. and Zheng, L. (2016), "Analytical solution of seismic stability against overturning for a rock slope with water-filled tension crack", *Geomech. Eng.*, **11**(4), 457-469.

GC